

5/9

SANDIA REPORT

SAND95-0885 • UC-706

Unlimited Release


Printed May 1995

Capacitive Sensor for High Resolution Weld Seam Tracking

Dan J. Schmitt, James L. Novak, Jimmie L. Akins

Prepared by
Sandia National Laboratories
Albuquerque, New Mexico 87185 and Livermore, California 94550
for the United States Department of Energy
under Contract DE-AC04-94AL85000

Approved for public release; distribution is unlimited.

 DISTRIBUTION OF THIS DOCUMENT IS UNLIMITED

Issued by Sandia National Laboratories, operated for the United States Department of Energy by Sandia Corporation.

NOTICE: This report was prepared as an account of work sponsored by an agency of the United States Government. Neither the United States Government nor any agency thereof, nor any of their employees, nor any of their contractors, subcontractors, or their employees, makes any warranty, express or implied, or assumes any legal liability or responsibility for the accuracy, completeness, or usefulness of any information, apparatus, product, or process disclosed, or represents that its use would not infringe privately owned rights. Reference herein to any specific commercial product, process, or service by trade name, trademark, manufacturer, or otherwise, does not necessarily constitute or imply its endorsement, recommendation, or favoring by the United States Government, any agency thereof or any of their contractors or subcontractors. The views and opinions expressed herein do not necessarily state or reflect those of the United States Government, any agency thereof or any of their contractors.

Printed in the United States of America. This report has been reproduced directly from the best available copy.

Available to DOE and DOE contractors from
Office of Scientific and Technical Information
PO Box 62
Oak Ridge, TN 37831

Prices available from (615) 576-8401, FTS 626-8401

Available to the public from
National Technical Information Service
US Department of Commerce
5285 Port Royal Rd
Springfield, VA 22161

NTIS price codes
Printed copy: A03
Microfiche copy: A01

DISCLAIMER

Portions of this document may be illegible in electronic image products. Images are produced from the best available original document.

Capacitive Sensor for High Resolution Weld Seam Tracking

Dan J. Schmitt
Intelligent System Sensors and Controls Department

James L. Novak
Microsensor Research and Development Department

Jimmie L. Akins
Computer-Aided Manufacturing Department
Sandia National Laboratories
Albuquerque, New Mexico 87185

Abstract

A non-contact capacitive sensing system has been developed for guiding automated welding equipment along typical v-groove geometries. The Multi-Axis Seam Tracking (MAST) sensor has been designed to produce four electric fields for locating and measuring the v-groove geometry. In this system, the MAST sensor is coupled with a set of signal conditioning electronics making it possible to output four varying voltages proportional to the electric field perturbations. This output is used for motion control purposes by the automated welding platform to guide the weld torch directly over the center of the v-groove. This report discusses the development of this capacitive sensing system. A functional description of the system and MAST sensor response characteristics for typical weld v-groove geometries are provided. The effects of the harsh thermal and electrical noise environments of plasma arc welding on sensor performance are discussed. A comparison of MAST sensor fabrication from glass-epoxy and thick-film ceramic substrates is provided. Finally, results of v-groove tracking experiments on a robotic welding platform are described.

*This LDRD Final Report is provided under Contract 3513110.

SC
DISTRIBUTION OF THIS DOCUMENT IS UNLIMITED

Acknowledgments

The authors would like to thank Phil Fuerschbach and Jim Bullen of the Physical and Joining Metallurgy Department (1831) for their technical input to this project, and for the use of their plasma arc welding equipment.

Contents

1.	Introduction.....	6
2.	System Components	6
2.1	Capacitive Sensing Technology	6
2.2	Signal Conditioning Electronics.....	8
3.	Sensor Design and Fabrication.....	9
3.1	Electrode Tip Design Strategies	11
3.2	Strategy Modification for Thick Film Fabrication	12
4.	Environmental Considerations for Welding	13
5.	System Calibration.....	18
6.	Sensor Simulated and Experimental Characteristics.....	21
7.	Robotic Welding Experiments.....	24
7.1	Robotic Hardware and Sensor Interface	24
7.2	Seam Tracking Experiments.....	26
8.	Conclusions	29
	References.....	30

Figures

1	The Multi-Axis Seam Tracking Sensor.....	7
2	Diagram of the Multi-Axis Seam Tracking Sensor	8
3	MAST Sensor Principle of Operation.....	9
4	Signal Conditioning Electronics	10
5	Electrical Schematic of the MAST Sensor.....	11
6	Sensor Capacitances	12
7	Side-Looking Sensor Output With 250 Amp Variable Polarity Welding	15
8	Effect of DC Weld Current on MAST Sensor Output (No Part Motion)	15
9	Effect of DC Weld Current on MAST Sensor Output (With Part Motion).....	16
10	Baseline Sensor Output (No Welding)	17
11	Side-Looking Sensor Output With 20 Amp Variable Polarity Welding	17
12	Typical V-Groove Geometry	18
13	Scan Directions for Calibration	19
14	Y Axis Calibration Data at Various Heights Above 3/16" V-Groove.....	19
15	Comparison of Y Axis Calibration Data for Various V-Groove Sizes.....	20
16	Down-Looking Sensor Data at Various Heights Above 3/16" V-Groove	20

17	Scan Directions for MAST Sensor Experiments to Compare Experimental and Model Data.....	22
18	Comparison of Simulated and Experimental Output of Down-Looking Sensors.....	22
19	Comparison of Phase Differences Between Down-Looking and Side-Looking Sensors for a Distance of 1 mm Above the Test Fixture Surface.....	23
20	Robotic Arc Welding System.....	24
21	Hobart Advanced World Control System II (HAWCS II)	25
22	MAST Sensor Interfaced With Welding Torch and Wire Feeder Guide	26
23	System Block Diagram	27
24	Sensor Output During Real-Time Tracking of 1/4" V-Groove While Welding.....	28
25	Welded V-Groove	28

Tables

1	MAST Sensor Thermal Tests.....	14
---	--------------------------------	----

Acronyms

AC	alternating current
A/D	analog to digital
DC	direct current
HAWCS II	Hobart Advanced World Control System II
I/O	input/output
LDRD	laboratory-directed research and development
MAST	Multi-Axis Seam Tracking
OD	outer diameter
PCB	printed circuit board
PID	proportional, integral, derivative
RAIL	Robot Automatix Incorporated Language
VME	versa module Europe
VP	variable polarity

Capacitive Sensor for High Resolution Weld Seam Tracking

1. Introduction

Large classes of manufacturing operations require the precise tracking of a gap or seam between mating parts. This is particularly true in the field of welding. In automated welding machines, precision fixturing of the parts is often required to hold the weld joints in precise location. Such precision means that preprogrammed trajectories can be executed by the motion equipment. While this is successful in some applications, several difficulties can arise. As welding is a thermally active process, thermal deformation of the plates can cause weld-joint locations to change. Also, small-lot manufacturing operations can make it prohibitively expensive to manufacture the precision fixturing required to locate the weld joint precisely. As a result, weld seam tracking sensors are often required to guide the automated welding equipment along the weld joint geometry.

As parts are being processed, seam-tracking sensors provide the error signals that the manipulator uses to follow the desired seam accurately in real-time. These data are fed back to the machine controller that modifies the nominal trajectory to compensate for mismatch in the joint, misalignment of the fixture, and process-induced distortions of a workpiece. Thus, a wide variety of "disturbances" can be rejected by the control system. This results in a useful processed part. Seam tracking sensors permit automation and robotics to be applied to small-lot welding operations at a cost-effective rate.

This report focuses on how a noncontact Multi-Axis Seam Tracking (MAST) sensor can be used in an automated welding system. The MAST sensor is simple, low in cost, requires little maintenance, and can be readily applied to a variety of automated seam-tracking or feature-tracking problems. Because it does not come into contact with the weld plate, the sensor can locate weld grooves more quickly, thereby reducing the time required for processing. This report describes the MAST sensor's principle of operation and response characteristics around typical weld v-groove geometries. Experiments that tested the MAST sensor's ability to survive in the thermal and electrical environment associated with welding are discussed. Sensor fabrication methods are also discussed. Finally, experiments in real-time weld seam tracking on a robotic platform are reviewed.

2. System Components

2.1 Capacitive Sensing Technology. A unique, noncontact capacitive sensing technology that locates and measures objects has been developed and patented.¹ A MAST sensor based on this technology has been designed. The sensor is easily used to locate key features on a weldment and to track the weld seam geometries in real-time.² Figure 1 is a photograph of the sensor; Figure 2 is a diagram of the sensor.

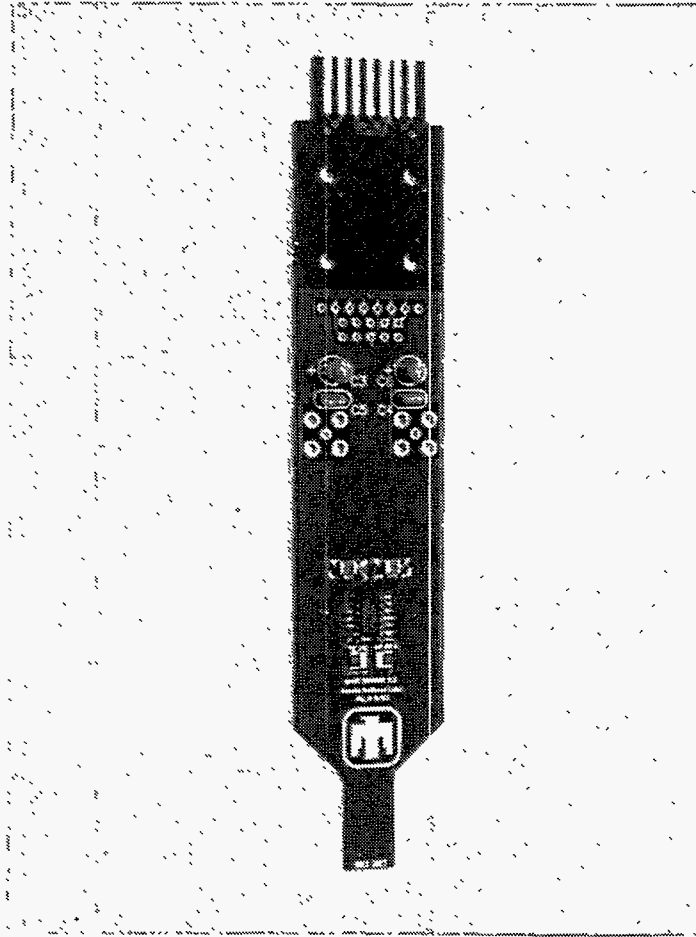


Figure 1. The Multi-Axis Seam Tracking Sensor

The MAST sensor is fabricated from an inexpensive, multi-layer printed circuit board (PCB) and is ~ 15-cm long and 2.5-cm wide. The tip of the sensor consists of four capacitor electrodes that provide tracking information in the Δy and Δz directions, and the $\Delta \rho$ orientation (rotation about y). Sensor signals are carried to signal conditioning electronics by a cable connected to the edge connector located opposite the tip.

The MAST sensor generates four electric fields that are affected by changes in sensor position relative to the weldment. Changes in the electric fields are detected as capacitance variations and are converted to voltage changes by the signal conditioning electronics. These electric fields are shown in Figure 3.

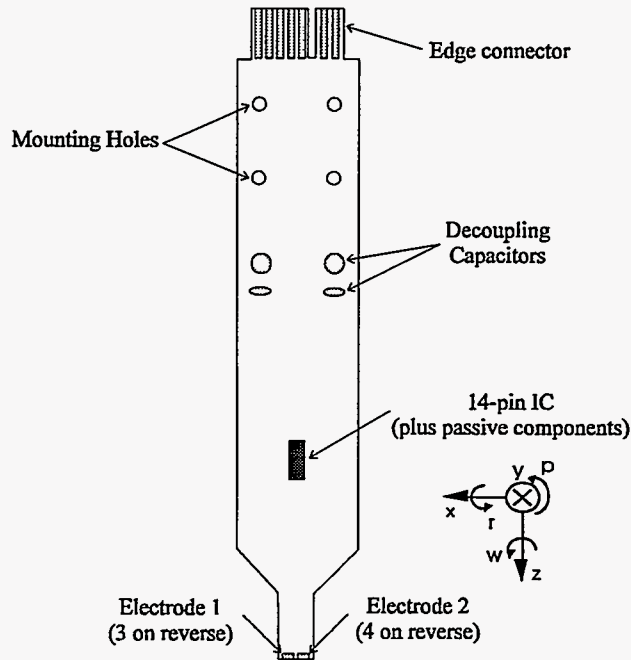


Figure 2: Diagram of the Multi-Axis Seam Tracking (MAST) sensor

Figure 3a shows the MAST sensor positioned directly over a typical weld v-groove. Two "side-looking" fields are shown associated with electrode pairs 1-2 and 3-4. When the sensor is directly over the v-groove as shown, the voltage associated with the fields is equal. As the sensor and v-groove become misaligned, there is an imbalance in the voltages associated with these fields. The magnitude of the difference between these voltages is proportional to cross-groove (y) displacement, while the sign of the difference indicates the direction (+y or -y) of misalignment.

Figure 3b shows a cross-sectional view of the MAST sensor positioned over the v-groove. Two "down-looking" fields are formed between electrode pairs 1-3 and 2-4 (into the page). The sum of the voltages associated with these fields is proportional to the distance above the groove (z). The difference between the voltages is proportional to the orientation relative to the cross-groove (y) axis.

2.2 Signal Conditioning Electronics. A set of signal conditioning electronics is located remotely from the robot arm. These electronics provide the driving signals for the MAST sensor and process the return signals to provide an analog output to the robot controller. Figure 4 shows a photograph of the signal conditioning electronics. The signal conditioning electronics consist of three boards mounted in a chassis. An oscillator board generates the driving frequencies and reference signals for the individual channels of the MAST sensor.

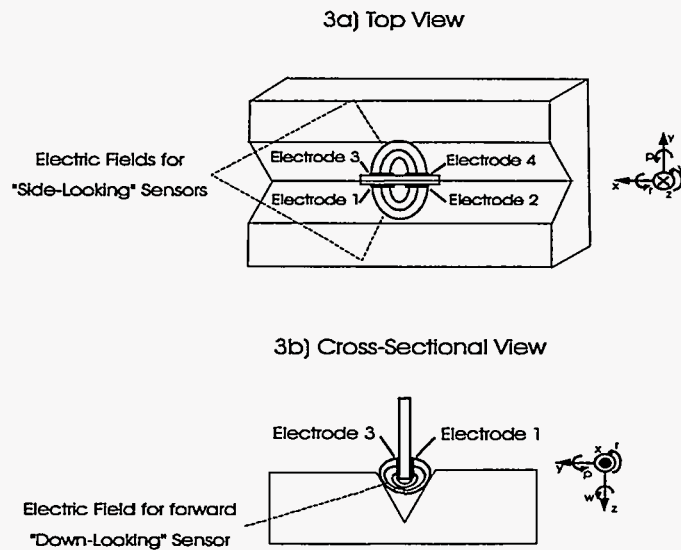


Figure 3. MAST Sensor Principle of Operation (The top view illustrates "side-looking" fields while the cross-sectional view illustrates "down-looking" fields)

To avoid coupling between channels, two separate frequencies in the 100 kHz range drive the four MAST channels. A synchronous detection board processes the return signals from the MAST sensor to provide analog output to the robot controller. The system outputs four varying voltages, which can be read directly into the robot controller through analog to digital (A/D) converters. A personality board provides the required interconnections between the synchronous detection board and the oscillator board to drive the MAST sensor.

3. Sensor Design and Fabrication

MAST sensor technology uses multiple, spatially directed electric fields for multi-axis position measurement. These electric fields interact with the workpiece to produce capacitance changes that are measured using a synchronous detection technique.

The electrical schematic for the MAST sensor is shown in Figure 5. Two different frequency oscillator signals are connected to Electrodes 2 and 3. Electrodes 1 and 4 are positioned such that four capacitors are formed in spatially distinct directions. The displacement currents between electrodes are converted to an output voltage via the op amp and the feedback capacitor. The outputs of these charge amplifiers consist of the sum of two amplitude-modulated signals at the two driving frequencies. By detecting the amplitudes of the two frequencies separately using synchronous detectors, signals corresponding to the sensor capacitance value can be obtained. In Figure 5, for example, the amplitude of frequency component f_1 at the output of the upper charge amplifier corresponds to the capacitance between Electrodes 1 and 2. Similarly, the f_2 amplitude corresponds to the capacitance between Electrodes 1 and 3.

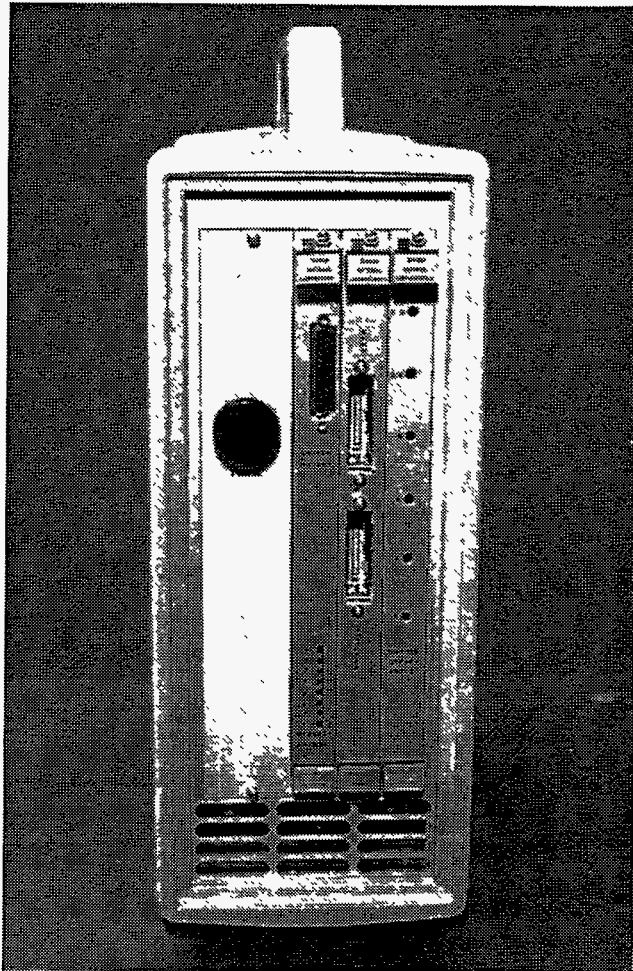


Figure 4. Signal Conditioning Electronics

In the actual sensor layout, there are a number of undesirable capacitances that may exist between the sensor electrodes or the interconnecting traces. Because the sensor positional resolution is limited by the smallest capacitance changes that can be measured, it is critical to optimize the sensor electrode shape and conductor layout to enhance sensitivity while reducing the effect of parasitic capacitances.

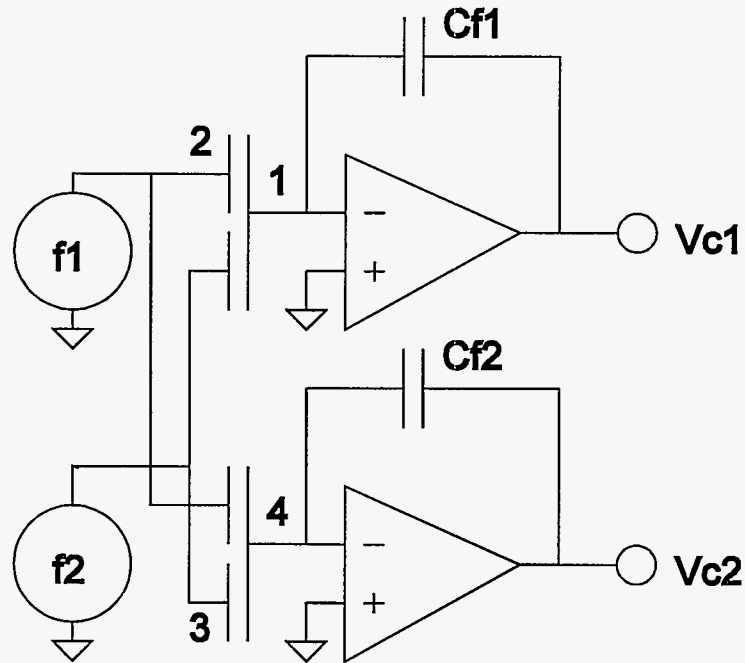


Figure 5. Electrical Schematic of the MAST Sensor

3.1 Electrode Tip Design Strategies. As indicated in Figure 3, the MAST sensor incorporates four electrodes to generate four independent electric fields. The shape and the spacing of the electrodes determines the spatial orientation of the corresponding field. However, the measured capacitance is actually the parallel combination of a sensor capacitance (C_{12}), which varies with distance from the workpiece, an interlayer parasitic capacitance (C_{ip}), and a parasitic free-space capacitance (C_{free}). (See Figure 6.) To enhance the sensitivity, the parasitic capacitances must be reduced to the degree that the desired change in the sensor capacitance represents a larger fraction of the total measured capacitance.

The interlayer parasitic capacitance can be reduced by placing a ground plane beneath the electrodes. Minimizing the thickness of the dielectric between the electrodes and the ground plane minimizes the interlayer parasitic capacitance due to a shielding effect. Reducing this layer also increases the capacitance from the electrodes to ground. Because the charge amplifier configuration results in a virtual ground at Electrodes 1 and 4 (see Figure 5), capacitances to ground from any of the electrodes or their interconnecting traces do not affect the MAST sensor sensitivity. Nevertheless, these capacitances must be considered since they increase by tens of picofarads the electrical load the oscillator must drive.

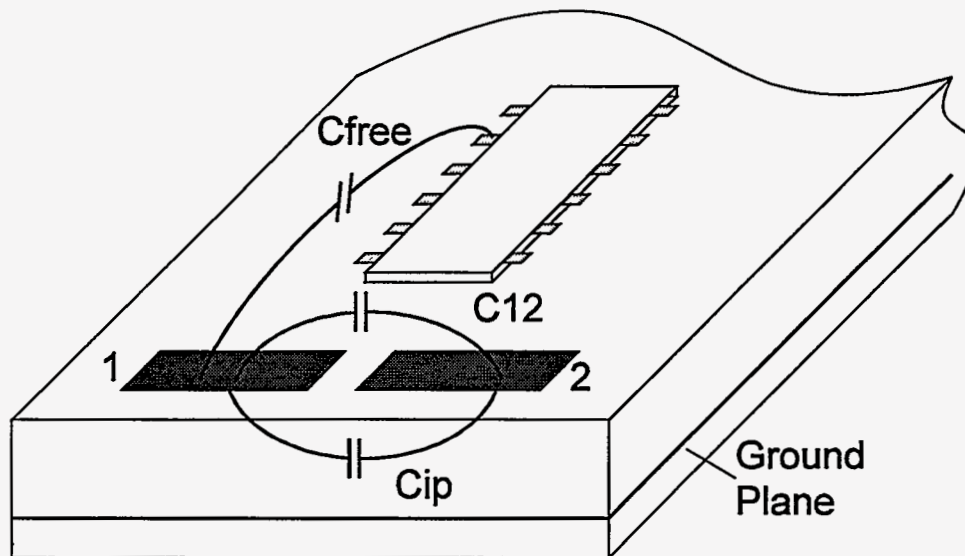


Figure 6. Sensor Capacitances

The free-space parasitic capacitance occurs between the sensor electrodes and any direct path between electrical connections to either of the oscillators. Care must be taken either to shield the oscillator cabling or to prevent cabling from moving in the space adjacent to the electrodes or charge amplifiers. Additionally, it is critical to ground any shielding adequately, because a floating shield will become capacitively coupled to the oscillator line. Note that a human hand holding an unshielded ribbon cable can produce large amounts of free-space coupling that will disrupt all measurements.

The feedback capacitances in the charge amplifier circuits determine the gain of the sensor. Because these are relatively small (~ 2 pF), the interlead and intertrace capacitances between the op amp output and inverting input stages can appreciably alter the nominal design gain. It is important to lay out traces so that conductors that connect the feedback elements in the two charge-amplifier stages are identical. Even differences in the volume of solder used to connect the components can alter the uniformity of sensor gain across charge amplifiers.

3.2 Strategy Modification for Thick-Film Fabrication. The strategies described above are important in fabricating MAST sensors using glass-epoxy or FR4 substrates. As part of this laboratory-directed research and development (LDRD), Sandia also attempted to fabricate sensors using thick-film technology on ceramic substrates.

Ceramic fabrication of the MAST sensor could extend high-temperature operation. It would do so at the expense of additional brittleness and susceptibility to breaking upon unintentional contact with the workpiece. By incorporating fired ink resistors and interdigitated electrode capacitors, it should be possible to use laser trimming to equalize

charge-amplifier gains. By locating the integrated circuit further from the electrodes and possibly incorporating a heat-shielding tube, the MAST sensor can be used in welding, plasma cutting, and other high-temperature operations.

However, Sandia efforts at fabricating ceramic, thick-film sensors met with only limited success. The thick-film process is an additive one; each screen printing builds up an additional layer. Since printed-circuit-board (PCB) fabrication is subtractive, the conductor layers designed for a PCB cannot be directly copied to a thick-film design. A different set of designs is required to produce screens suitable for multi-layer thick-film fabrication.

The blind vias used in PCB fabrication are difficult to construct using thick-films. These vias provide the interlayer shielding required for optimal operation. In our experiments, most of the three-hole blind vias on the ceramic sensors were electrically shorted to the ground planes. In addition to thick-film problems, it is difficult to manufacture symmetrical ground planes because of the relative thicknesses of the ceramic substrate and the fired-ink dielectric layers.

4. Environmental Considerations for Welding

In order to become a functional sensor for welding applications, the MAST sensor must survive and it must supply functional data during the harsh environment created by the welding process. Of concern is the MAST sensor's capability to survive the high temperature and high electromagnetic noise environments generated by the welding process. Tests to evaluate the MAST sensor's performance in these environments were conducted.

MAST sensor testing was performed using two automated plasma arc welding setups. Initial testing was performed on a research system in Department 1831. This system consists of a plasma arc welding torch deployed from a stationary position, and a welding power supply. Part motion was achieved with a set of x-y stages for providing translation in two directions. Tests on the system consisted of mounting the sensor at varying distances from the weld torch and executing a variety of weld and motion schedules.

Subsequent testing was performed on the HAWCS II robotic arc welding system described in Section 7. These tests had the MAST sensor mounted at a fixed distance of 1.75 inch from the weld torch. Our primary concern in these tests was to evaluate MAST sensor performance in:

1. the thermal environment of welding
2. the noise generated during pilot arc initiation
3. the noise generated during dc welding
4. the noise generated during variable polarity (ac) welding.

To evaluate the thermal survivability of the PCB version of the MAST sensor, the sensor was mounted at distances varying from 1 inch to 6 inches from the center of the weld torch. Weld current maximums were:

- 50 amps in the direct current mode and 45 amps (at 6 inches from torch) in the variable polarity mode on the Department 1831 system
- 250 amps in the variable polarity mode on the HAWCS II system.

Table 1 summarizes the minimum distance and maximum amperage tests for each system. The sensor successfully survived the thermal environment associated with all these tests with no degradation in output. Figure 7 shows evidence of this for the test run on the HAWCS system at 1.75 inch distance from the torch with 250 amps weld current in the variable polarity mode. The figure shows a test that traverses down the length of the part while welding. Plotted is the sensor signal formed by subtracting the two side-looking readings. This is the signal used for seam tracking purposes. The fact that the sensor output returns to its baseline level at the end of the test is evidence the sensor has survived the thermal environment. The noise levels shown in Figure 7 are discussed in Section 7.

Table 1: MAST Sensor Thermal Tests

Distance from Torch (inches)	Weld Current (amps)	Current Mode	Result	System
1	20	vp	Pass	Department 1831
1	50	dc	Pass	Department 1831
1.75	250	vp	Pass	HAWCS II

Effects of the electromagnetic noise generated during pilot arc initiation and dc welding were evaluated on the Department 1831 welding setup. Figure 8 shows the output from all four sensor channels during pilot arc initiation and dc welding at 35 amps with no torch motion. The sensor was mounted 6 inches from the torch for this test. Pilot arc initiation occurred during the first second of the test. No effect is seen on the sensor output. Weld arc initiation occurred at 13 seconds into the test. A small noise spike can be seen on Channel 3. The weld arc was extinguished at 23 seconds into the test. Small noise spikes can be seen on Channels 1, 2, and 3. The dc welding current had no significant effect on the sensor output. Figure 9 shows the same test conditions with part motion. Sensor signals are observed to decrease as the sensor moves along the test part, and then increase at motion reversal. This is due to the system tracking the sensor away from the seam center. (No sensor-based motion control was performed on the system in these evaluations.) At motion reversal, the weld arc is extinguished and the sensor is guided back across the welded section. By comparing the output with weld torch on and off we observed that the dc welding current had no significant effect on the sensor output.

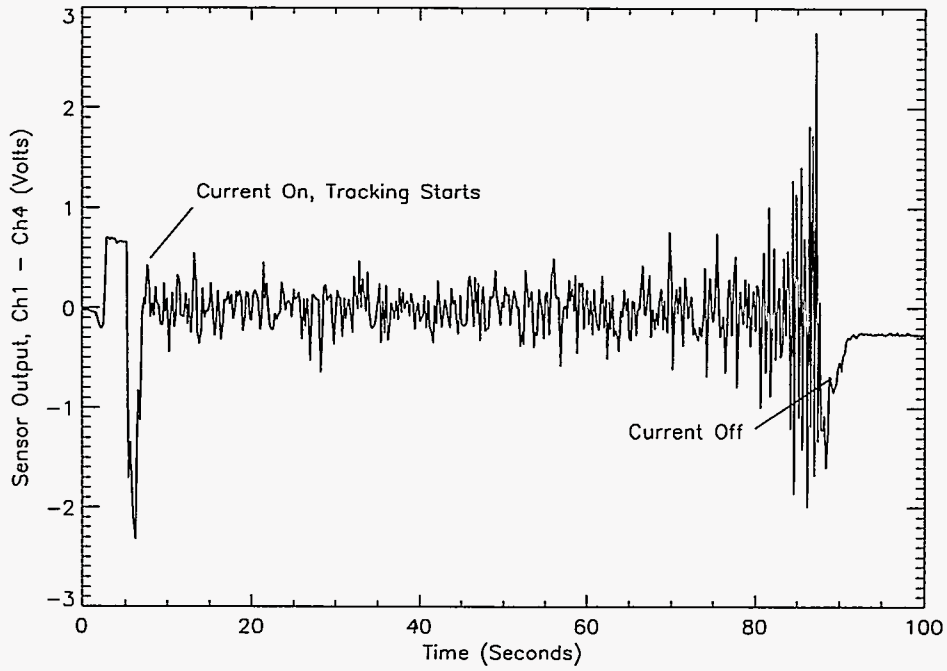


Figure 7. Side-Looking Sensor Output With 250 Amp Variable Polarity Welding

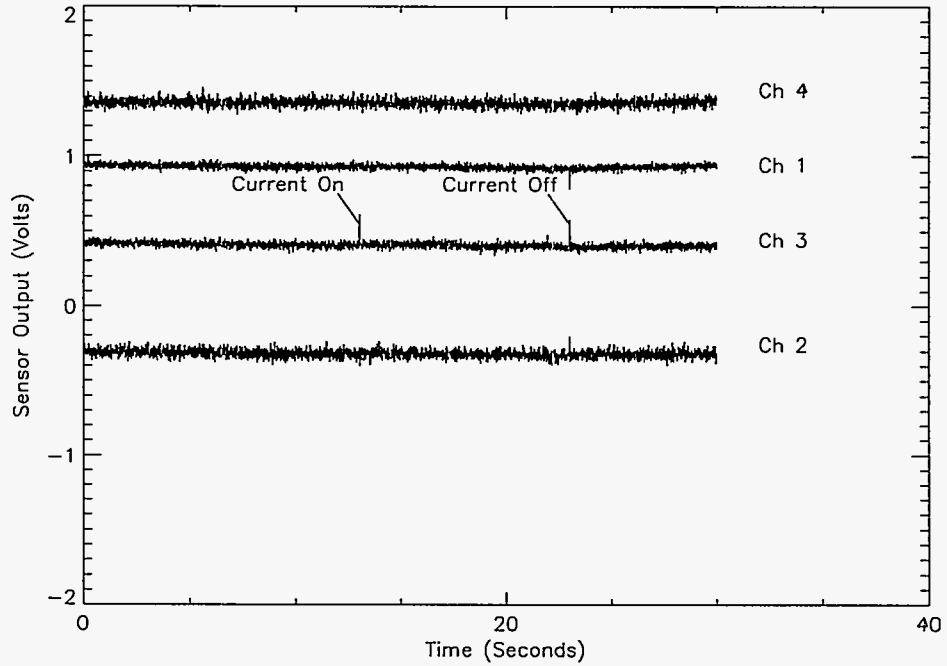


Figure 8. Effect of DC Weld Current on MAST Sensor Output (No Part Motion)

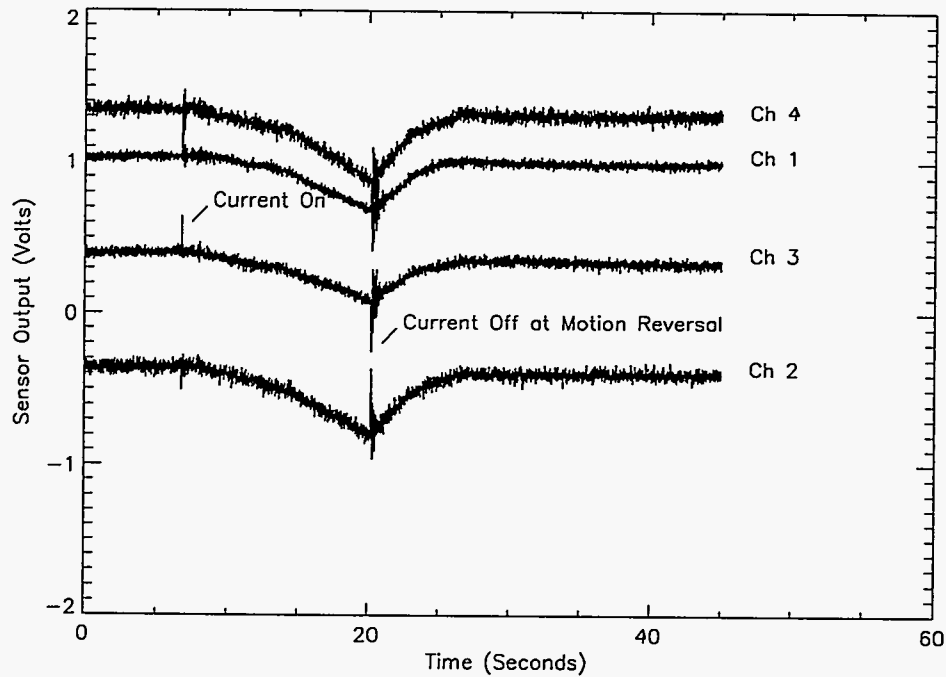


Figure 9. Effect of DC Weld Current on MAST Sensor Output (With Part Motion)

Effects of the electromagnetic noise generated during variable polarity (ac) welding were more significant in the early evaluation. Figures 10 and 11 document testing on the Department 1831 system by comparing the output of the side-looking channels without and with weld current, respectively. Plotted is the difference between side-looking channel readings, which is the signal used for seam tracking purposes. Test conditions for this run were 20 amps weld current with the sensor mounted 1 inch from the weld torch. In both tests, the sensor was guided along the test part with motion reversal at the end. The sensor was then guided back over the previous section. This section of the test depicted in Figure 11 had been welded.

Comparison of the plots shown in Figures 10 and 11 shows a significant coupling of the noise generated by the variable polarity mode of welding into the sensor output. The resulting output was unacceptable for seam tracking. This demonstrates the need for improving proper grounding connection between the MAST sensor system and the welding system, and for improving signal filtering within the MAST signal conditioning electronics. As no seam tracking experiments were planned for this system, no attempts were made to resolve the noise problem on this test setup. The improved output of the MAST sensor system on the HAWCS robotic system is discussed in Section 7.

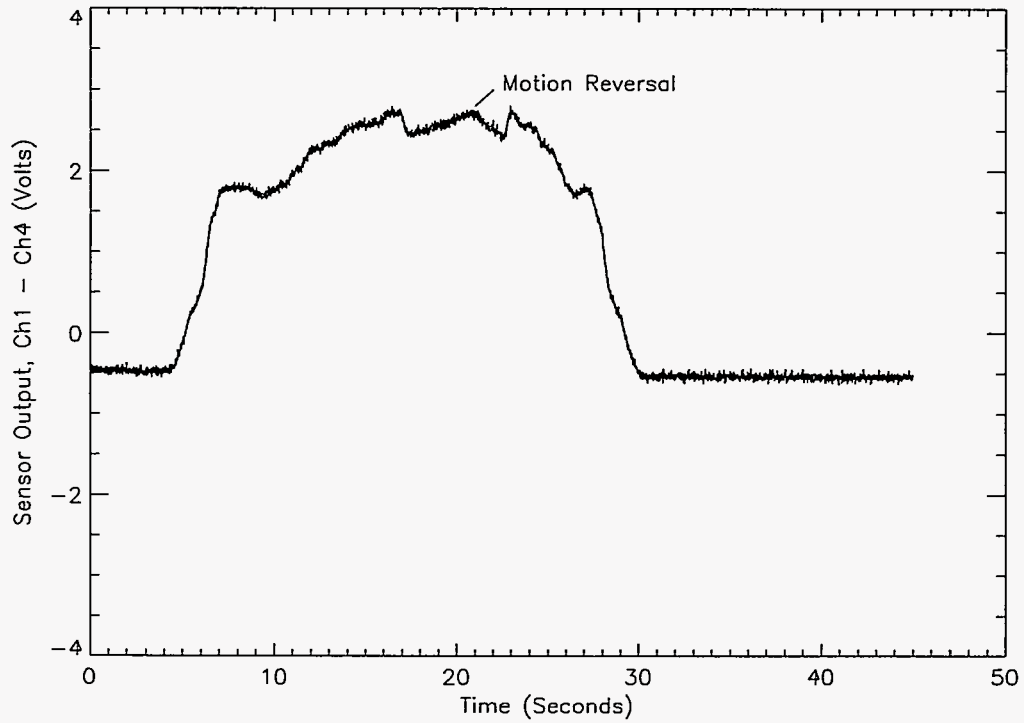


Figure 10. Baseline Sensor Output (No Welding)

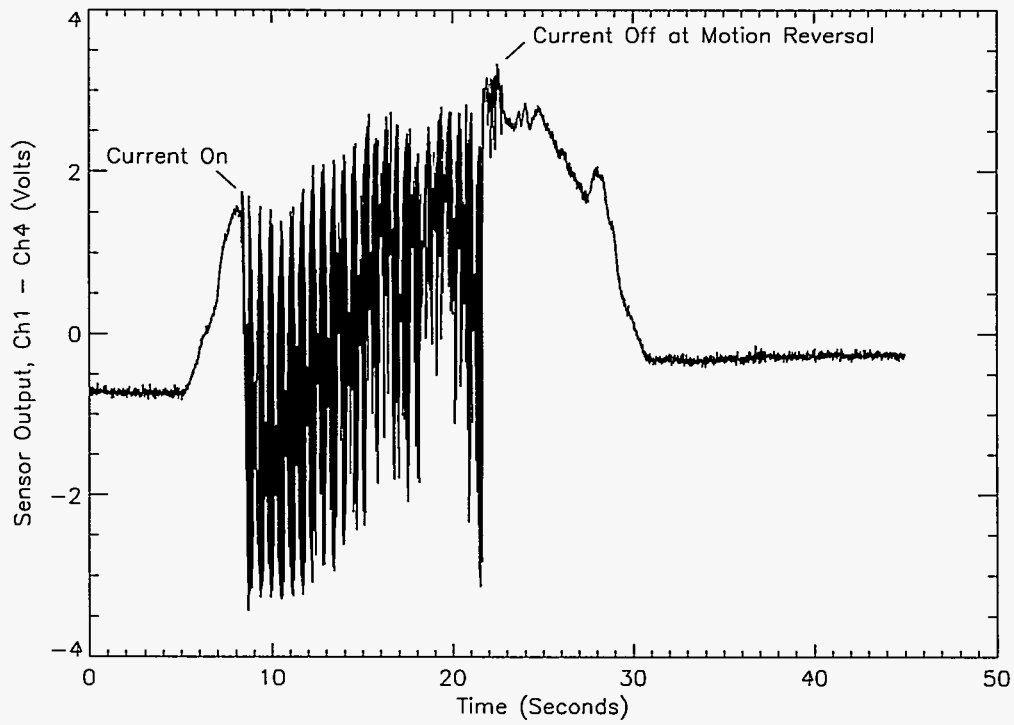


Figure 11. Side-Looking Sensor Output With 20 Amp Variable Polarity Welding

5. System Calibration

The incoming MAST sensor signals are calibrated with respect to the weld v-groove geometry. Calibration is required so that these signals, in A/D counts, can be converted to absolute distances with respect to the v-groove. Calibration data was collected for a range of v-groove sizes to examine the sensitivity of the sensor to size variation. Figure 12 shows the typical v-groove geometry and the range of sizes we examined.

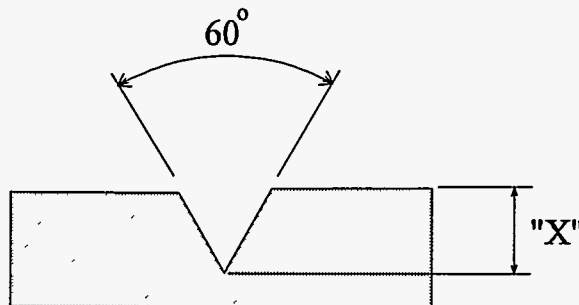


Figure 12. Typical V-Groove Geometry. (Sizes examined: X [inches] = 5/16, 1/4, 3/16, 1/8, 1/16.)

Calibration involved scanning the MAST sensor across the v-grooves to obtain data for both the y and z axes (see Figure 13). Figure 14 shows data collected for scans in the y direction at various z heights above the 3/16" v-groove. Plotted is the difference between the two side-looking sensors, (1-2) minus (3-4). The plot shows a single-period signal that crosses zero at the point of symmetry corresponding to the v-groove center. The magnitude of the signal decreases as the z scan height increases. Figure 15 compares the sensor output at a 1 mm scan height for the 5 cross-sections shown in Figure 13. Figure 16 shows the data collected for down-looking sensor (1-3) at various heights above the 3/16" v-groove. This signal reaches a minimum value at the location that corresponds to the v-groove center. The signal characteristic for the other down-looking sensor (2-4) is identical to that shown in Figure 16.

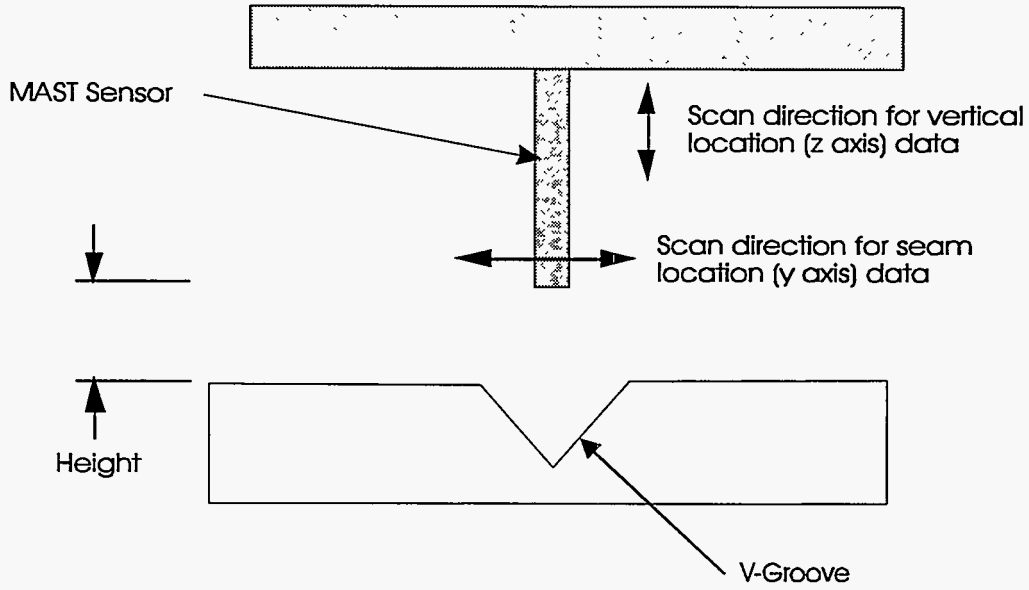


Figure 13. Scan Directions for Calibration

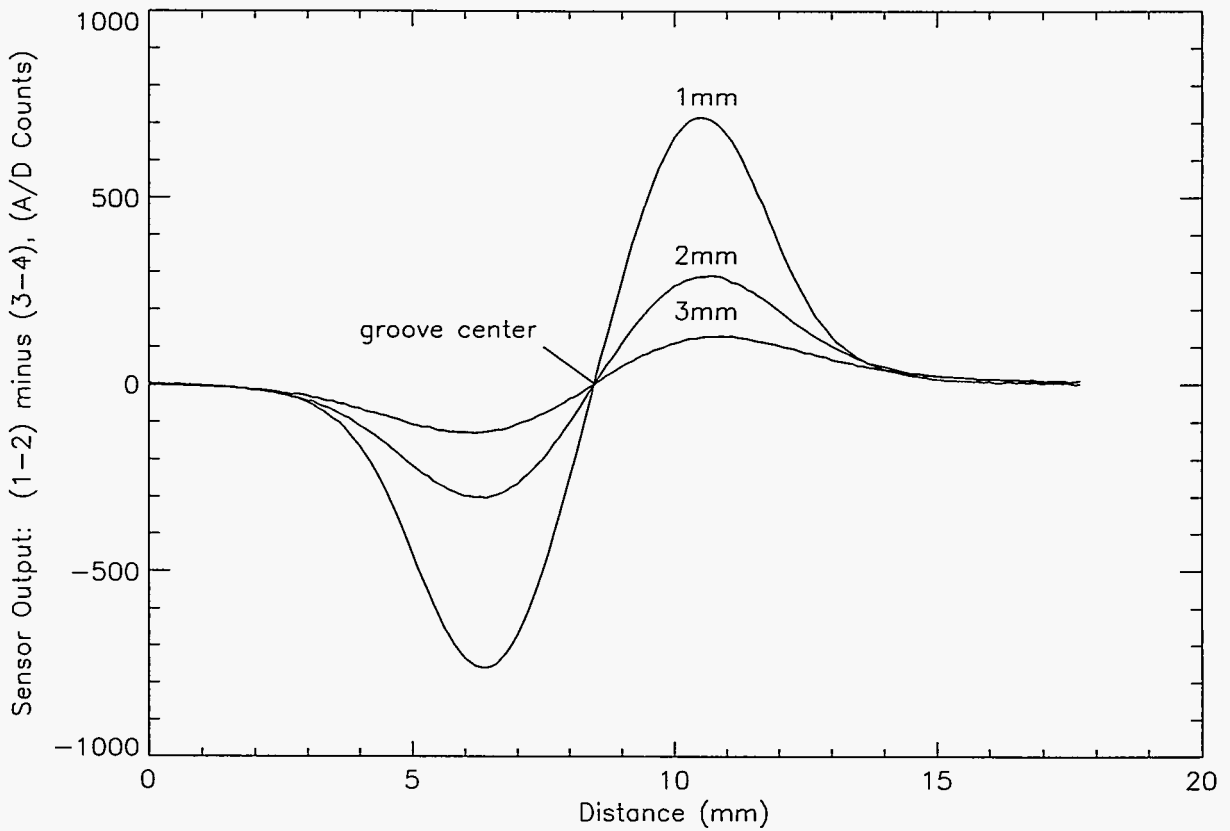


Figure 14. Y Axis Calibration Data at Various Heights Above 3/16" V-Groove

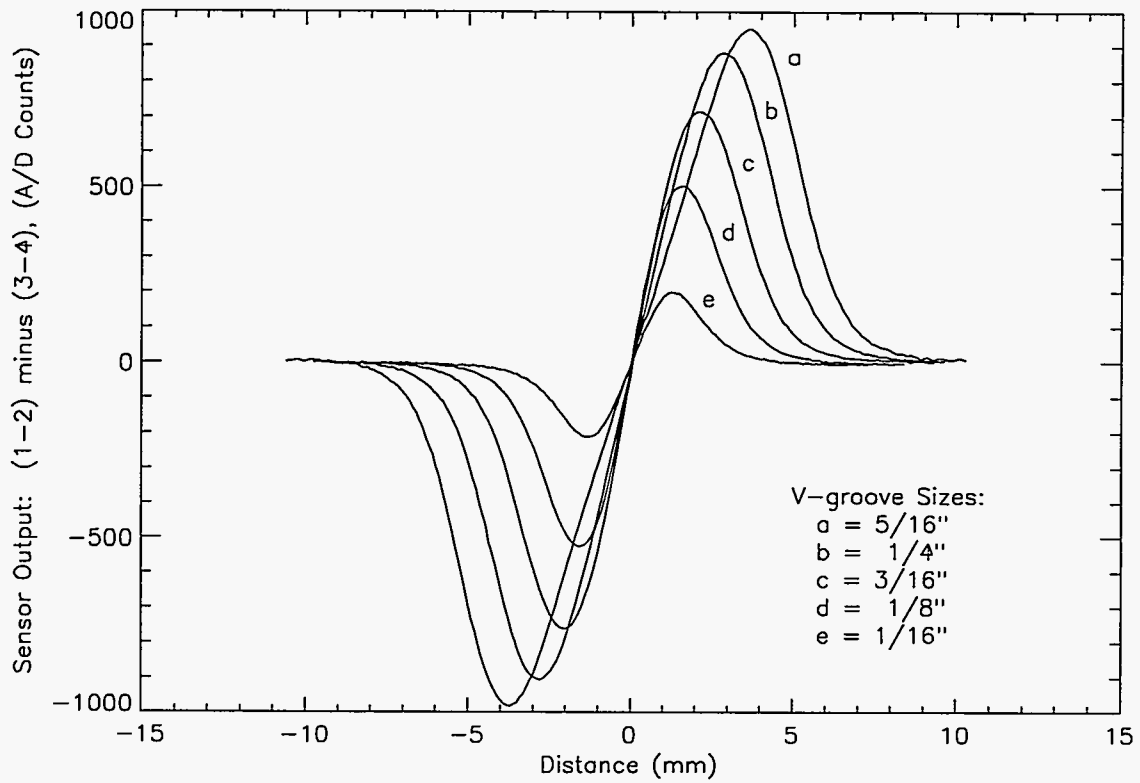


Figure 15. Comparison of Y Axis Calibration Data for Various V-Groove Sizes

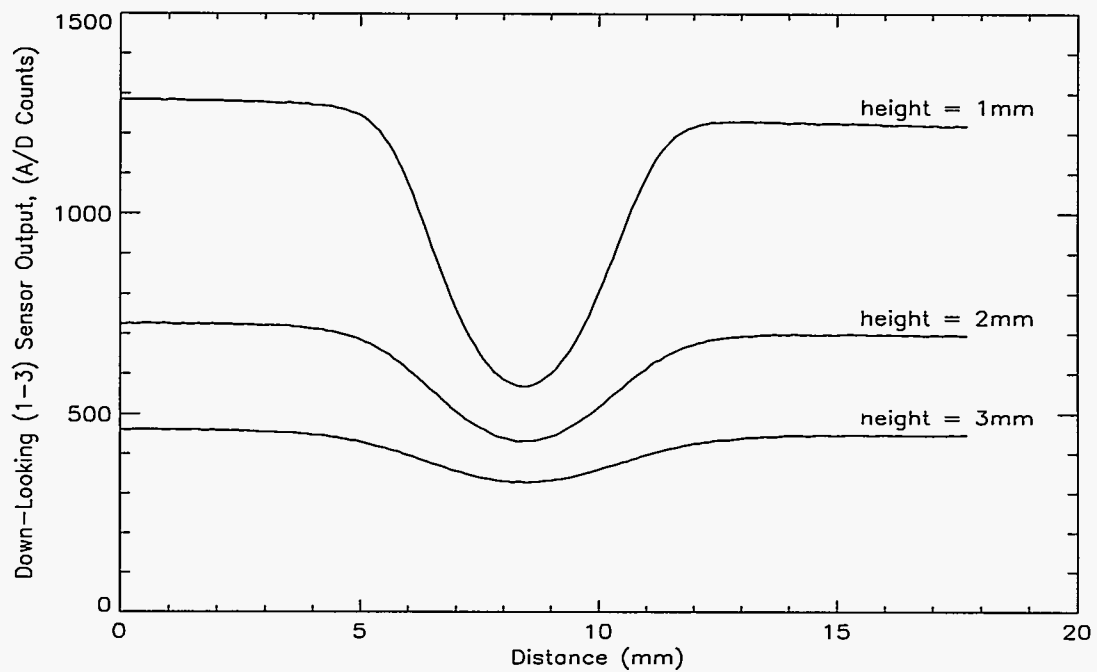


Figure 16. Down-Looking Sensor Data at Various Heights Above 3/16" V-Groove

Our strategy in real-time seam tracking is to use MAST output to position the sensor directly over the v-groove center before tracking begins. Assuming that seam-tracking is reasonably accurate, the sensor will remain in the vicinity of the groove center near the zero crossing (see Figure 14). Since the slope of the sensor output is approximately linear near the zero crossings, a linearized gain can be used to represent the y-axis behavior. The seam tracking experiments discussed in this report were conducted at a tracking height of 1 mm above the v-groove top surface.

Calibration parameters were also determined for controlling the height (z) above the groove during tracking. This calibration was performed by placing the sensor directly over the groove and varying the distance from the groove. In the z direction, the down-looking sensor signal decreases monotonically as height z increases. A linearized calibration gain was obtained by approximating the slope of the z axis sensor output at the 1 mm desired tracking height.

6. Sensor Simulated and Experimental Characteristics

The down-looking MAST sensors were simulated in 2D using the Electro[©] boundary element software package. The simulated sensor was "moved" across a surface. (See Figure 17 where the surface is represented by a cross section of a series of 9.5 mm OD tubes.) The mutual capacitance between the down-looking electrodes was calculated for different sensor distances from the gap between the tubes. The data are plotted as solid lines in Figure 18. As expected, the signals are at a maximum when the sensor is directly over the gap. This is explained by the fact that the shielding effect of the tubes on the sensor electric fields is at a minimum at this position. As the sensor is moved further from the gap toward the top surface of a tube (distance = 4.25 mm), the signals reach a minimum value of capacitance as the shielding effect increases.

The MAST sensor was experimentally tested using a fixture consisting of a flat bundle of 9.5 mm OD tubes. The sensor tip was oriented parallel to the seam axis as indicated in Figure 17. Data values were collected as the sensor was moved perpendicularly to the bundle surface in the y axis (across the gaps) for 1 and 2 mm heights (above the surface). Data from the down-looking sensors is plotted (as symbols) versus distance from the tube gap for two different nominal heights (in z) above the nozzle bundle in Figure 18.

The minimum and maximum values of the experimental data have been linearly scaled to match the simulated values. Notice that the model accurately predicts the shape of the response curves throughout the nonlinear profile. Because the electric fields extend primarily along the z-axis, the down-looking sensors exhibit a greater sensitivity to changes in this distance than do the side-looking sensors. This is noticeable in Figure 18 where the dynamic range of the signal at 2 mm above the surface is significantly smaller than that for a 1 mm distance. These down-looking sensors are primarily used to control the motion of the robot toward the test fixture or weld plate surface.

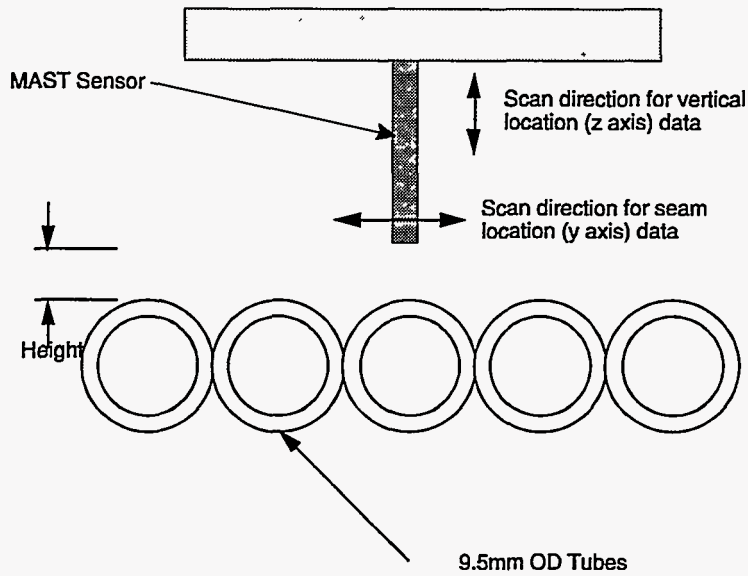


Figure 17. Scan Directions for MAST Sensor Experiments to Compare Experimental and Model Data

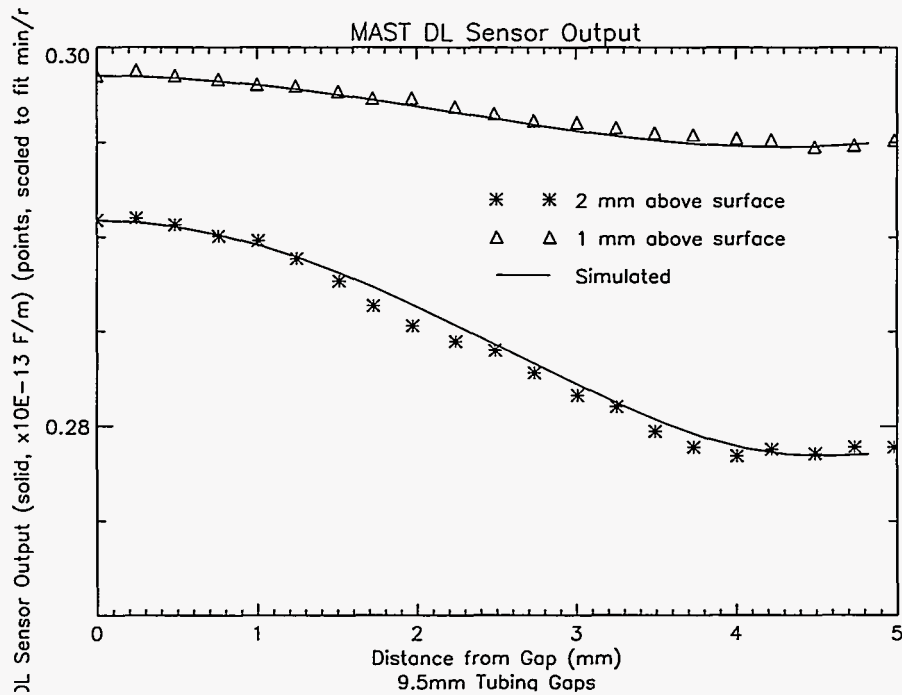


Figure 18. Comparison of Simulated and Experimental Output of Down-Looking Sensors.

Figure 19 shows a plot of the two side-looking sensor signals, their difference, and a down-looking sensor output as the sensor was scanned along the y axis of the tube bundle at a distance 1 mm above the surface. Notice the phase differences between the signals. The down-looking sensor signals are in phase with the gap, rising to a maximum at the gap location. The value of the difference signal goes to zero at both the centers of the seams and at the tops of the tubes due to the symmetrical geometry at both locations. The sum of side-looking sensor signals, SL12 and SL34 (not shown in Figure 19), exhibit positive peaks at locations over the tops of tubes and negative peaks at seams. Thus, the difference signal identifies the locations of symmetry, while the sum of the sensor signals identifies whether the location is a tube top or a seam. This sensor information is used to locate a seam precisely by directing the robot to drive the sensor tip to zero. This will balance the readings of the side-looking sensors by making them equal to zero. The sensor tip is driven to zero while maintaining a minimum value for the common-mode side-looking sensor signal.

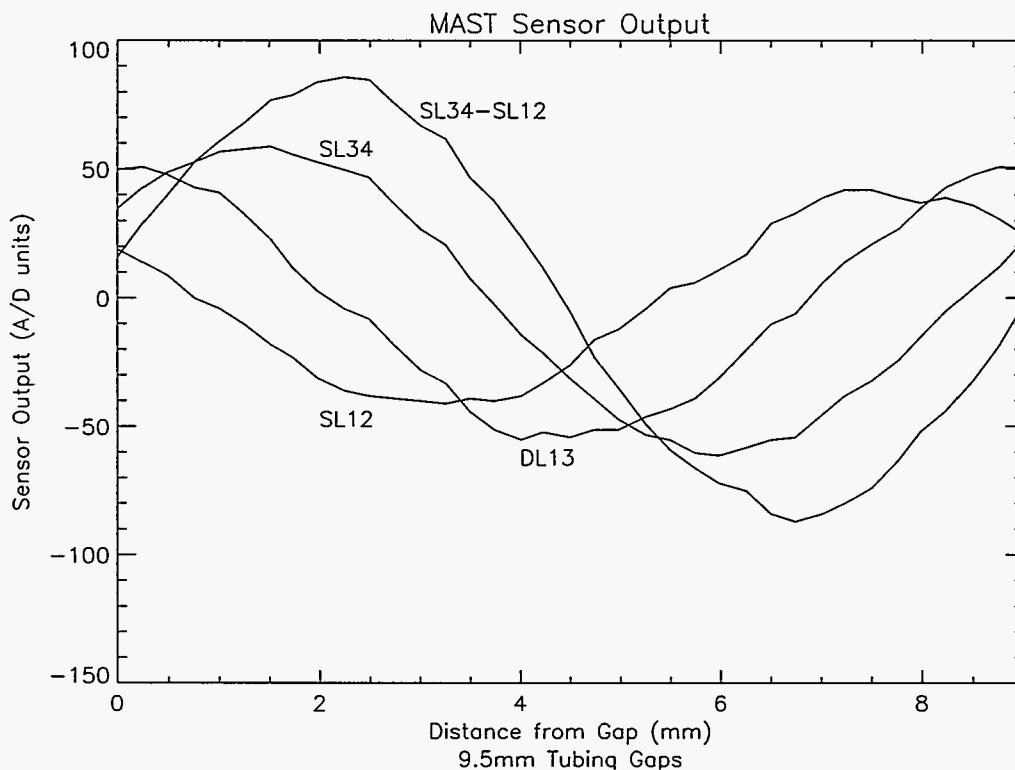


Figure 19. Comparison of Phase Differences Between Down-Looking and Side-Looking Sensors for a Distance of 1 mm Above the Test Fixture Surface.

7. Robotic Welding Experiments

7.1 Robotic Hardware and Sensor Interface. The MAST sensor system was interfaced to a robotic arc welding system so that experiments in seam-tracking of typical weld v-groove geometries in real-time could be conducted. The robotic arc welding platform is shown in Figure 20. System components include a Motoman K-30 robot. This articulated, 6 degree of freedom robot is capable of lifting 30 kg (66 lbs.). A plasma arc welding torch and wire feed guide is deployed from the tool face plate. The welding power supply is a Hobart Advanced Systems variable polarity power supply. The system provides welding currents of up to 300 amps. The currents can be supplied in both the dc and the variable polarity (ac) modes. A gas and water circulation system circulates cooling water to the torch and controls the flow of plasma and shielding gas to the welding torch. Cooling water is provided from a closed-loop radiator system. The entire system is controlled from the Hobart Advanced World Control System (HAWCS) II shown in Figure 21. This is a VME-based controller that provides integrated control over the welding process, robot motion, and the gas and water circulation system. Application software is developed in the RAIL programming language.

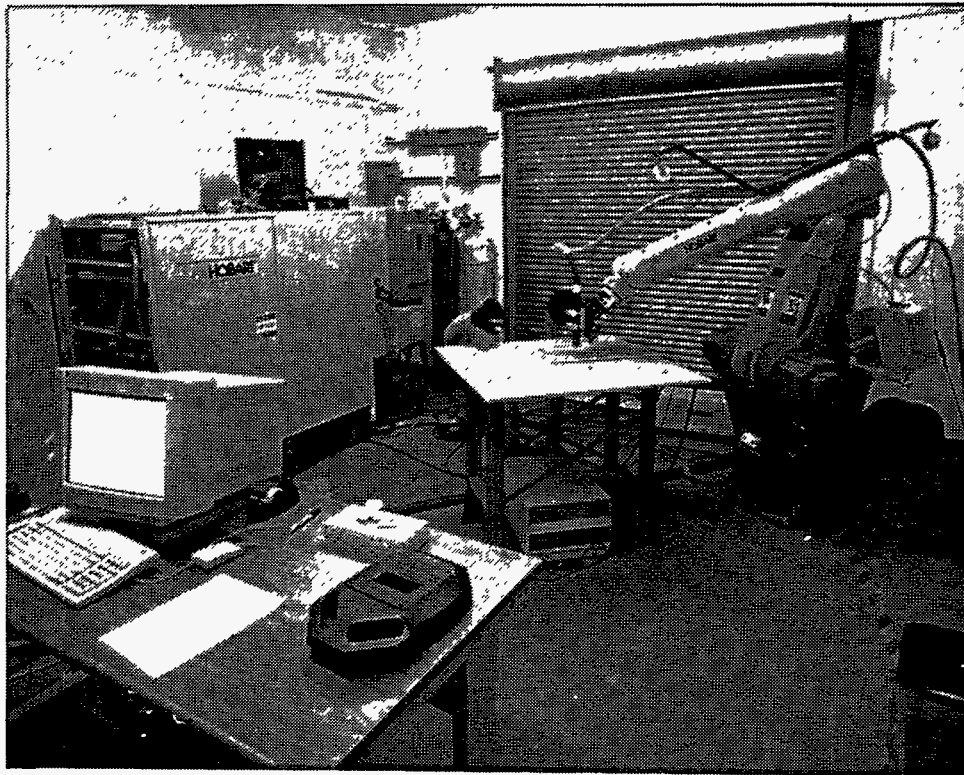


Figure 20. Robotic Arc Welding System

The MAST sensor was interfaced with the welding torch and wire guide feeder on the end of the robot arm as shown in Figure 22. The sensor was mounted at ~ 1.75 inches from the center of the plasma welding torch and positioned so that the guide could feed cold wire to the leading edge of the weld pool. The sensor mounting was electrically isolated from the welding torch and the guide. This provided proper grounding and eliminated the coupling of electromagnetic noise from the variable polarity mode of welding as discussed in Section 6. The signal conditioning electronics were positioned outside the robot's workspace. To repeat, considerable attention was given to the grounding of these electronics with respect to the welding power supply to reduce noise coupling from the welding process.

Figure 21. Hobart Advanced World Control System II (HAWCS II)



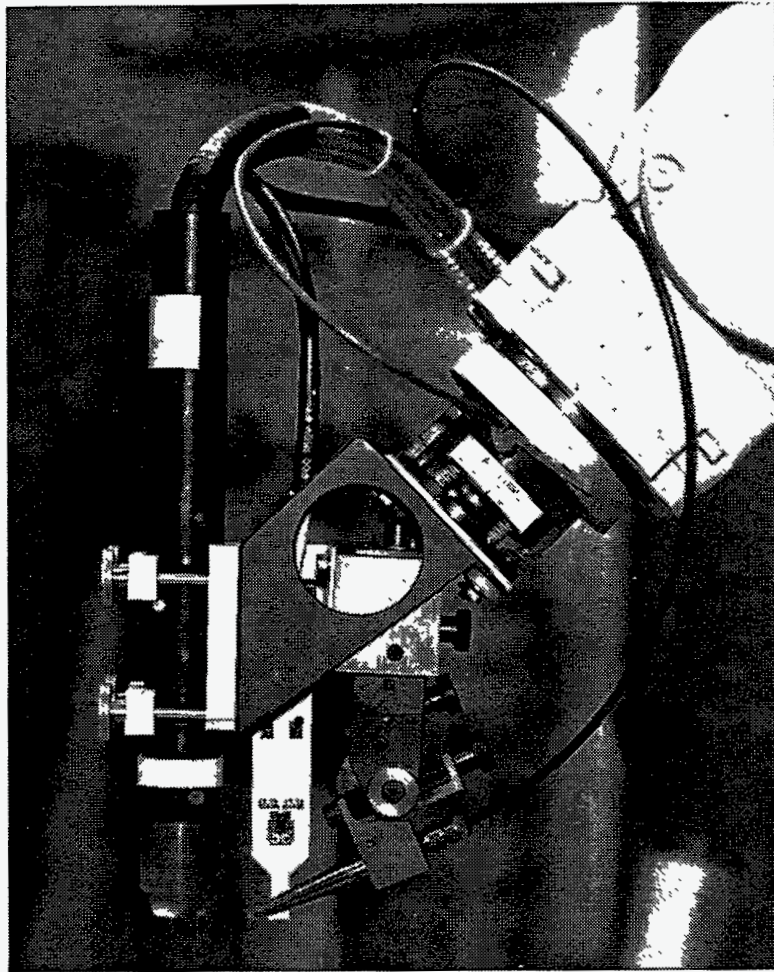


Figure 22. MAST Sensor Interfaced With Welding Torch and Wire Feeder Guide

7.2 Seam Tracking Experiments. Seam tracking experiments were conducted to demonstrate that the MAST sensor system was capable of tracking weld v-grooves in real-time while welding with weld wire feed. Output from the MAST sensor was used in real-time to guide the robot and welding equipment along the seam. Real-time seam tracking required that Sandia design a control system capable of producing a fast, stable response from the robotic equipment. Figure 23 shows the system block diagram for the cross-seam regulation system where the difference between the two side-looking sensors was driven to zero. In this system, a proportional, integral, derivative (PID) control algorithm acts on the error signal to generate a position command for the robot. The resulting robot motion positions the MAST sensor with respect to the weld v-groove. Misalignment between the sensor tip and the groove center results in a tracking error that is measured by the MAST sensor. The sensed tracking error is fed back to form the error signal that is to be driven to zero.

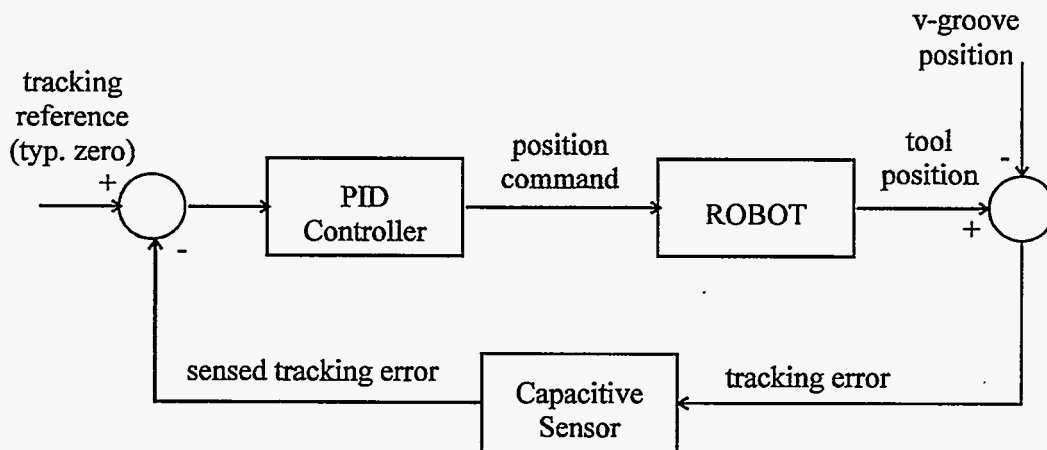


Figure 23. System Block Diagram

Real-time seam tracking on the HAWCS II system was accomplished by using a system-provided, low-level, real-time offset package. This package provides the user access to PID filters with user selectable gains. The PID filter operates on a user-defined error signal and attempts to drive the error to zero. A HAWCS II concept called I/O Points is used to define the error signal. These points are updated at a rate of 20 Hz.

A series of experiments was conducted that ultimately demonstrated the system's ability to track a 1/4" v-groove during variable polarity welding at 250 amps current. The variable polarity pulse was 19 msec forward current and 4 msec reverse current. The tracking speed was 2.5 mm/sec. Figure 24 shows output from this tracking experiment. Plotted in this figure is the difference between the two side-looking sensors: CH1 - CH4. The control system attempts to drive this error signal to zero. Weld-current initiation and seam tracking began at ~ 8 seconds into the tests. Figure 24 shows that some noise did couple into this sensor output, but the signal was sufficient for successful tracking of the seam. Figure 25 shows a photograph of the welded v-groove.

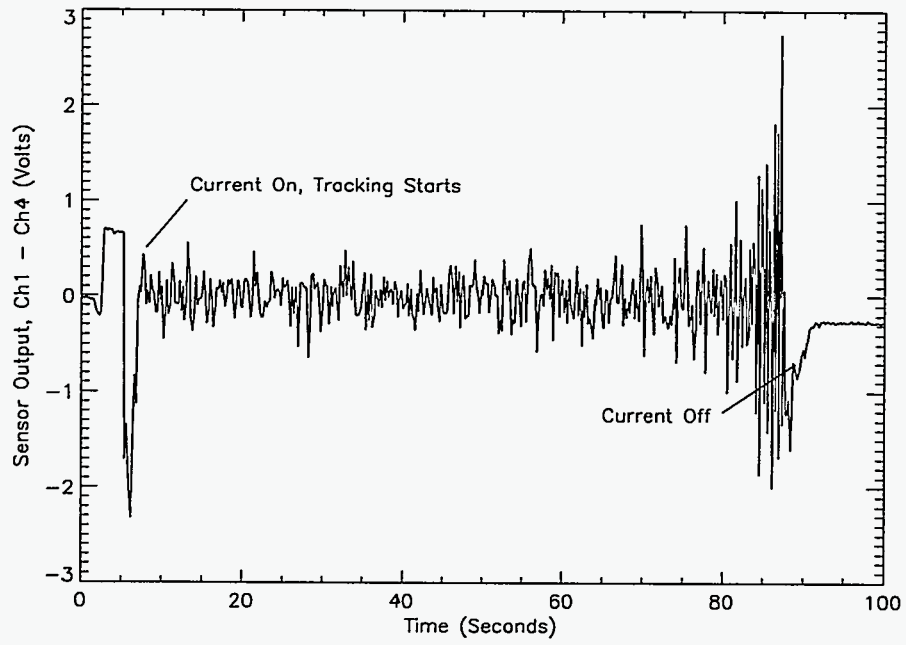


Figure 24. Sensor Output During Real-Time Tracking of 1/4" V-Groove While Welding



Figure 25. Welded V-Groove

8. Conclusions

This report has covered the successful development of the MAST sensor as a viable weld seam tracking system. We have demonstrated that the sensor can survive in the harsh environment associated with welding, and provide output that can be used by the motion control system for successfully tracking weld v-groove geometries.

Issues that will require continued investigation are the electromagnetic noise environment generated by the variable polarity mode of welding. While it has been successfully demonstrated that coupling of this electromagnetic noise into the sensor's signal condition electronics can be reduced to sufficient levels for successful v-groove tracking, the consistency with which this noise is reduced needs to be improved. The current implementation relies heavily on proper grounding between the signal conditioning electronics and the welding equipment. Noise levels that result from the grounding will be influenced by how equipment is rearranged. Consistent guidelines for the proper relative placement of the electronics and ground connections need to be established. This is important because it affects the extent to which this technology will influence other automated welding platforms.

Additional investigations into the fabrication of MAST sensors using thick-film technology on ceramic substrates need to be conducted. Our efforts in this study demonstrate that current sensor designs for thin-film fabrication techniques did not translate well to thick-film fabrication techniques. Continued thick-film studies could resolve current problems and yield suitable designs. The technology would benefit from improved high-temperature sensor performance, since the improvement would mean that the MAST sensor could be physically located closer to the weld torch.

Several other improvements in the area of sensor technology need to be investigated before a fully functional weld seam tracking sensor is viable. The implementation discussed in this report concentrates only on symmetrical v-grooves. The seam tracking strategies currently used rely on this symmetry by tracking to the zero error point that corresponds to the seam location. However, other joint geometries (such as lap and bevel joints) will require different strategies for tracking the torch at the proper joint location. In this report, we have also focused on straight grooves. While the current configuration of the MAST sensor will successfully track grooves with large radius of curvatures, these radius of curvature limits need to be determined. Furthermore, new sensor electrode geometries will be required for an even smaller radius of curvatures. Finally, weaving of the weld torch to create the proper molten weld pool geometries is also a common welding practice. However, moving the torch also causes the MAST sensor to move relative to the joint. Strategies for processing the resulting sensor signals to determine the seam location need to be developed.

References

1. J. L. Novak, "Feature Tracking Impedance Sensor," U.S. Patent Application, 1993.
2. D. Schmitt, J. Novak, J. Maslakowski, G. Starr, "Sensor-Based Control of Rocket Thrust Chamber Feature Location for Automated Braze Paste Dispensing," Proceedings of the 1994 SME Fifth World Conference on Robotics Research, 1994, Cambridge, MA, September 1994, pp. 6-17 through 6-28.

Distribution

1	MS0320	LDRD Office, 1011
5	MS0351	J. L. Novak, 1315
5	MS0561	J. L. Akins, 2483
2	MS0949	P. A. Molley, 2111
25	MS0949	D. J. Schmitt, 2111
1	MS9018	Central Technical Files, 8523-2
5	MS0899	Technical Library, 13414
1	MS0619	Print Media, 12615
2	MS0100	Document Processing, 7613-2 For DOE/OSTI